PAPER
Alexander B. Cook *et al.*
Matrix metalloproteinase responsive hydrogel microplates
for programmed killing of invasive tumour cells

Check for updates

Matrix metalloproteinase responsive hydrogel microplates for programmed killing of invasive tumour cells†

Alexander B. Cook, [ID] *‡ Annalisa Palange, Michele Schlich, [ID] Elena Bellotti, Sayanti Brahmachari, Martina di Francesco and Paolo Decuzzi

Interactive materials are an emerging class of systems that can offer control over response and adaptivity in polymer structures towards the meso- and macroscale. Here, we use enzyme regulated cleavage of peptide crosslinkers in polymer hydrogels to release a cytotoxic therapeutic nanoparticle with an adaptable mechanism. Hydrogel microplates were formed through polyethylene glycol/peptide photoinitiated thiol−ene chemistry in a soft-lithography process to give square plates of 20 by 20 μm with a height of 10 μm. The peptide was chosen to be degradable in the presence of matrix metalloproteinase 2/9 (MMP-2/9). The hydrogel material's mechanical properties, swelling, and protease degradation were characterised. The microfabricated hydrogels were loaded with docetaxel (DTXL) containing poly(DL-lactide-co-glycolide) (PLGA) nanoparticles, and characterised for enzyme responsivity, and toxicity to MMP-2/9 overexpressing brain cancer cell line U87-MG. A 5-fold decrease in EC$_{50}$ was seen compared to free DTXL, and a 20-fold decrease was seen for the MMP responsive microplates *versus* a non-degradable control microplate. Potential applications of this system in post-resection glioblastoma treatment are envisioned.

Introduction

Glioblastoma multiforme is one of the most devastating and deadly forms of cancer.[1,2] Its extremely invasive nature and the currently limited treatment options mean that current survival is on average 15 months from diagnosis. Although its prevalence is relatively low, with approximately 2–3 new cases per 100 000 people per year, its poor prognosis makes it a critical public health concern.[3] Currently, recommended treatment involves surgical resection, and then oral chemotherapeutic temozolomide (TMZ), often combined with radiotherapy.[4] This combination has been shown to be the most effective current option, with 6 weeks of radiotherapy (60 Gy), together with concomitant chemotherapy with TMZ (75 mg m^{-2} daily), followed by six months of TMZ treatment (150–200 mg m^{-2} for 5 days every 28 days), now being standard.[5]

Complete resection *via* surgical methods is not possible due to the diffuse nature of the disease, and desire to leave unaffected brain cells untouched. In addition, oral and/or systemic therapies are severely limited by the blood brain barrier.[6] Typically, the tumour recurrence occurs within 2 cm of the original margins. This has led to the development of implantable devices for local and sustained drug delivery in the post operative tumour bed.[7,8] While these systems have led to improvements in patient survival, it has also been noted that polymer embedding can have disadvantages. The most widely used implantable system for GBM treatment are the clinically accepted Gliadel wafers, which are 1 cm polymer disks of poly((1,3-bis(carboxyphenoxy)propane)-co-sebacic acid), containing Carmustine chemotherapeutic. A systematic review from Komotar *et al.* of 19 studies and 795 patients receiving Gliadel treatments, showed 25% of patients experiencing seizures due to implant complications, and 12% of patients experiencing cerebral edema.[9] Patients receiving treatment with Gliadel wafers also had increased risk of intracranial infection and cyst formation associated with the non-natural biomaterials surface.[10] The large size and flat surfaces of Gliadel implants limit contact with residual tumour cells as they metastasise, while the polymer rigidity is not matched to the mechanical properties of the surrounding tissue.

Hydrogels are soft materials formed from the crosslinking of hydrophilic polymer chains, have water contents of typically >90%, and storage moduli higher than their corresponding loss moduli.[11,12] Advances in engineering of hydrogels with controlled size, shape, stiffness, and chemical functionality,

Laboratory of Nanotechnology for Precision Medicine, Istituto Italiano di Tecnologia, Via Morego, 16163 Genova, Italy. E-mail: a.b.cook@tue.nl

‡Present address: Bio-organic chemistry group, Department of Chemical Engineering and Chemistry, 5600 MB Eindhoven, Netherlands.

has allowed for increased application of these materials in areas such as tissue engineering, drug delivery, neural interfacing materials, and soft robotics.[13–15] The use of hydrogels as injectable or implantable local drug depots is becoming more widespread. Compared to *in situ* formed gels, pre-injection engineering of hydrogel materials allows more precise control over crosslinking, stiffness, and drug or nanoparticle loading.[16] This pre-administration materials engineering strategy has recently been used to great effect to produce drug delivery systems that can conform and adapt to the tumour resection cavity.[17] In addition, this strategy does not require UV irradiation directly on the brain which can damage healthy cells.[18]

Here, we have designed hydrogel microplates with tunable size and stiffness, formed through thiol–ene photoadditions of norbornene functional polyethylene glycol (PEG) and peptide crosslinkers, utilizing incorporated cysteine residues. The peptide linkers are cleavable by metalloproteases (MMP-9 and MMP-2) which are overexpressed in the infiltrating tumour microenvironment.[19] Incorporation of this enzyme responsiveness should limit toxicity to healthy cells and achieve higher dose to invasive tumour margins and metastases. Chemotherapeutic docetaxel (DTXL) has been encapsulated in poly(lactic-*co*-glycolic acid) (PLGA) nanoparticles, which are entrapped in the hydrogel network, and released on exposure to MMPs. Physiochemical characterization of the engineered microplates was carried out with microscopy techniques and profilometry, while *in vitro* enzyme response was confirmed with both imaging and a drug release assay. Toxicity studies on U87-MG brain cancer cells were carried out *in vitro*, and the drug loaded microplates effect on cell viability investigated. The enzyme responsive docetxel-loaded microplates have been compared to their non-degradable equivalents, free docetaxel-containing nanoparticles, and free docetaxel. We propose these microplates as a protective layer over resected tumour site, which have minimal degradation and drug release without the specific enzymatic triggers excreted by infiltrating tumour cells, able to deliver dosages to glioblastoma tumour cells while leaving healthy cells less affected.

Experimental

Materials

Polyethylene glycol tetranorbornene (M_w 10 000 g mol^{-1}), 2-hydroxy-40-(2-hydroxyethoxy)-2-methylpropiophenone (Photoinitiator), poly(D,L-lactide-coglycolide) acid (PLGA, lactide : glycolide 50 : 50, M_w 38 000–54 000 g mol^{-1}), poly(vinyl alcohol) (PVA, M_w 31 000–50 000 g mol^{-1}), and dithiothreitol (DTT), were purchased from Sigma-Aldrich. MMP-2/9 cleavable peptide (CVPLS↓LYSGC) was purchased from Genscript. Collagenase type IV (MMP-2/9) was purchased from Gibco Life technologies. Docetaxel (DTXL) was purchased from Alfa Aesar. Polydimethylsiloxane (PDMS) (Sylgard 184) was purchased from Dow Corning Corp. 1,2-Distearoyl-*sn*-glycero-3-phosphoethanolamine-*N*-[carboxy(polyethylene glycol)-2000]

(sodium salt) (DSPE–PEG2k–COOH), and 1,2-dipalmitoyl-sn-*glycero*-3-phosphocholine (DPPC) were purchased from Avanti Polar Lipids. MTT reagent 3-(4,5-dimethyl-2-thiazolyl)-2,5-diphenyl-2*H*-tetrazolium bromide was purchased from Sigma-Aldrich. InnoZyme™ MMP-2/9 activity assay kit was purchased from Merck Millipore and used following the manufacturer's instructions. All other reagents were purchased from Sigma-Aldrich/Merck unless specified.

Hydrogel formation

Hydrogels were formed from solutions of PEG-norbornene and thiol functional peptide (1 : 1, thiol : ene molar ratio) at varying weight percentages, in deionized water with 0.05 wt% photoinitiator. The prepolymer solution was added to square (1 cm by 1 cm) templates and crosslinked with UV light (365 nm, 10 mW cm^{-2}) for 5 minutes. Equilibrium swelling ratio was determined, to give information about network structure, degree of cross-linking, as well as hydrophilicity. The gels were placed in vials with deionized (DI) water for 24 h. The hydrogel dimensions were measured, and the gels were weighed after excess buffer was removed using paper. The hydrogels were then lyophilized to obtain the dry weight of the gels. The swelling ratio based on hydrogel mass (Q_M) was calculated. $Q_M = M_S/M_D$. Where M_S is the hydrogel mass after swelling and M_D is the dry hydrogel mass. Q_M was further used to calculate the volume swelling ratio (Q_V). $Q_V = 1 + \rho_D/\rho_S (Q_M - 1)$. Where ρ_D is the density of the dry hydrogel (1.12 g cm^{-3} for PEG) and ρ_S is the density of the solvent (1 g cm^{-3} for water).[20] For mechanical testing, hydrogels swollen in deionized water for 24 hours were measured for their dimensions prior to mechanical testing. Uniaxial compression testing was performed on an 3365 Instron dynamometer, equipped with a 10 N load cell. Load was applied with 1 mm min^{-1} rate until approximately 30% deformation. Compression modulus was calculated from the linear region of the stress strain curve and is the average of 5 repetitions. The porous structures of the lyophilized hydrogels were observed using a JEOL JSM-6490LA scanning electron microscope (SEM).

Hydrogel degradation assay

Cuboid hydrogels (~1 cm by 1 cm) were formed from a 10 wt% pre-polymer solution and submerged in a buffer solution (50 mM HEPES, 10 mM CaCl$_2$) for 24 hours to reach equilibrium swelling. The gels were weighed after removing excess surface water droplets, and incubated with different concentrations of collagenase IV in buffer solution (50 mM HEPES, 10 mM CaCl$_2$) at 37 °C. Hydrogels were collected at different time points, the hydrated samples were weighed, and the enzyme solutions refreshed every 24 hours. Each time point was performed in triplicate. The assay was also performed for different stiffness hydrogels but with only one concentration of enzyme (50 nM). Percent mass loss is defined as: mass loss (%) = $(W_t - W_0)/W_0 \times 100$, where W_t is the gel weight at specified time points and W_0 is the mass measured at equilibrium swelling.

Microplate fabrication and characterisation

Hydrogel microplate fabrication proceeded following adaptation of our previously reported process.[21] A master template is fabricated from a silicon wafer with direct laser writing, giving a template with an array of square wells of 20 μm by 20 μm with a depth of 10 μm, with each well separated by 3 μm from the adjacent wells. A PDMS inverse template is formed from the master by covering with PDMS elastomer and crosslinker (10:1, volume ratio), the air bubbles were removed under vacuum, and the PDMS is cured at 80 °C for 3 hours. After removing the PDMS from the silicon, a PVA solution (10 wt% in DI water) is added on top of the pattern and placed in an oven at 60 °C for 2 hours. The resulting PVA film is a replica of the silicon master template, after removal from the PDMS. Solutions of 4 arm PEG-norbornene and thiol functional peptide (10 wt%, and 1:1 thiol:ene molar ratio) in ethanol with 0.05 wt% photoinitiator, were spread over the wells of the PVA film and then crosslinked with UV light (365 nm, 10 mW cm^{-2}) for 5 minutes. In the case of non-degradable microplates, the dithiol DTT was used in place of the peptide. The templates are then dissolved in DI water, and the released microplates collected by centrifugation at 1717g for 5 minutes, resuspending in DI water and centrifuging again. Microplate profile on a flat surface was measured with an optical profilometer (Zeta-20 from KLA-tencor). Average size and size distribution were obtained with a Multisizer 4 Coulter counter (Beckman Coulter) with a 100 μm capillary, and following guidance on particle measurement from the manufacturer's documentation. Scanning electron microscopy was performed from an air dried drop of microplates on silica, after uniform gold sputter coating, with a JEOL JSM-6490LA SEM Analytical (low-vacuum) scanning electron microscope (5–15 keV). Swelling volume change of the hydrogel microplates was estimated using optical microscopy. The microplates were allowed to swell in DI water for 24 hours, then imaged in solution (Leica 6000). A size distribution was determined using image-J analysis on approximately 100 particles, and the average microplate volume was calculated, and compared to the initial template dimensions to give an estimated volume swelling ratio of the microplates (fold change volume = V_f/V_i).

Microplate degradation assay

For degradation studies: after resuspending a batch of microplates in water, this microplate solution was evenly divided between pre-weighed Eppendorf tubes, centrifuged (1717g for 5 minutes) and the supernatant removed, then incubated with different concentrations of collagenase IV in buffer solution (50 mM HEPES, 10 mM CaCl$_2$) at 37 °C. The microplate samples were then centrifuged, and the supernatant was removed (1717g for 5 minutes), lyophilized, and weighed. Percent mass loss is defined as: mass loss (%) = $(W_t - W_0)/W_0 \times 100$, where W_t is the lyophilised microplate weight at specified time points and W_0 is the lyophilised microplate weight at time zero. Each time point corresponds to a separate Eppendorf and performed in triplicate. Microplate degradation

in different concentrations of collagenase IV was also confirmed with SEM (JEOL JSM-6490LA), and optical microscopy (Leica 6000), by similarly incubating with enzyme buffers at 37 °C, and imaging at determined timepoints.

Spherical polymeric nanoparticle (SPN) fabrication and characterisation

Spherical polymeric nanoparticles were fabricated using an oil-in-water emulsion method previously reported by our group and others. The oil phase consisted of PLGA (1 mg) and DPPC lipid (100 μg) dissolved in chloroform (450 μL). DTXL (200 μg) was also added to oil phase when required. This solution was added dropwise to 3 mL of 4% ethanol containing 110 μg of DSPE–PEG2k–COOH under probe sonication (1 min at 60% amplitude). The cloudy solution was stirred for 3 hours, until complete evaporation of organic solvent. The nanoparticles were purified through sequential centrifugation steps. Firstly, 5 min at 452 g to remove any possible large debris, and then the supernatant was centrifuged 3 more times for 20 min at 18 104g. Dynamic light scattering was used to characterize the size and zeta (ζ) potential of nanoparticles under aqueous conditions at pH 7.0 (Nano ZS, Malvern). DTXL loading and release kinetics were characterized with high-performance liquid chromatography (HPLC), in triplicate with equal amounts nanoparticles in separate Eppendorf microtubes for each time point. SPNs were separated from free drug by centrifugation at 18 104g. Acetonitrile and water were added to achieve 50:50 water:acetonitrile (to either the SPN pellet for loading calculation, or supernatant for release studies), in which the particles are dissolved and the DTXL can be resolved. Release studies were carried out with gentle shaking at 37 °C in 1 mL PBS, in order to have same volume and thus be comparable to microplate release assays. HPLC details: Agilent 1260 Infinity, equipped with a 100 μL sample loop injector, and C18 column (4.6 × 250 mm, 5 μm particle size, Agilent). DTXL is eluted under isocratic conditions using a binary solvent system [H$_2$O + 0.1% (v/v) TFA/AcN + 0.1% (v/v) TFA, 50:50 v/v] pumped at a flow rate of 1.0 mL min^{-1}. The UV detection is set at 230 nm and the retention time of DTXL is 3.09 min. An external standard curve in a linear concentration ranging from 1 to 200 μg mL^{-1} is used for the quantification of DTXL. Loading efficiency (weight percentage of the drug over the SPN weight) and encapsulation efficiency (ratio between the DTXL entrapped inside SPNs over the initial feeding amount) were determined.

Spherical polymeric nanoparticle (SPN) loading and drug release

The loading of nanoparticles (PLGA SPNs loaded with DTXL) into microplates is achieved via absorption. Briefly, microplates are first lyophilized, then allowed to re-swell in a small volume (50 μL, approx. 20 mg mL^{-1}) of concentrated nanoparticle solution, and finally washed with water and centrifuged to remove any nanoparticle excess (1717g for 5 minutes). Loading is performed at 1:1, w:w, overall weight ratio of nanoparticles to microplates. Loading efficiency (weight per-

© 2023 The Author(s). Published by the Royal Society of Chemistry

RSC Appl. Polym., 2023, **1**, 19–29 | 21

centage of the drug entrapped inside µPLs over the lyophilised µPL weight) and encapsulation efficiency (weight percentage of the DTXL entrapped inside µPLs over the initial feeding amount in SPNs) were determined. Loading and encapsulation efficiency was calculated in triplicate, by completely degrading the microplates in 500 nM collagenase at 37 °C for 24 hours, then measuring concentration of DTXL with HPLC (acetonitrile added, 50 : 50, v : v, to dissolve released PLGA SPNs). To assess the release profile of DTXL from the SPN-loaded microplates, microplates were added to PBS, or various concentrations of collagenase type IV (MMP-2/9) in buffer solution (50 mM HEPES, 10 mM CaCl$_2$), (1 mL; pH 7.4) and gently shaken at 37 °C. Equal amounts particles were added in separate Eppendorf microtubes, for each time point, in triplicate. After the appropriate amount of time the samples were centrifuged to pellet the SPN-containing microplates (1717g for 5 minutes) supernatant was removed, acetonitrile added to the supernatant (50 : 50, v : v, to dissolve released PLGA SPNs) and DTXL measured with HPLC. HPLC conditions were identical to the conditions described above for DTXL-SPN characterisation.

Cell culture and cytotoxicity

U87-MG cells were cultured in EMEM with 10% FBS and 1% penicillin/streptomycin. Cells were seeded in 96-well microplate at a density of 7.5×10^3 cells per well and incubated for 24 h, then treated with different concentrations (5 wells per treatment) of free DTXL, DTXL-SPNs, DTXL-MMP-µPLs (MMP responsive microplates containing DTXL-SPNs), and DTXL-µPL (non-degradable microplates containing DTXL-SPNs). The same amount of microplates without any entrapped DTXL-SPNs was also tested to assess the effect of the hydrogel polymers on cell viability (empty MMP-µPL, empty non degradable µPL). After 72 h the media was refreshed and the MTT reagent (3-(4,5-dimethyl-2-thiazolyl)-2,5-diphenyl-2H-tetrazolium bromide, Sigma) added for 3 h. Formazan crystals were dissolved in DMSO and absorbance was measured at a wavelength of 550 nm with background subtraction at 660 nm (Tecan). The percentage of cell viability was assessed according to the following equation cell viability (%) = (AbsT/AbsC) × 100 where AbsT is the absorbance of treated cells and AbsC is the absorbance of control (untreated) cells. EC$_{50}$ values were calculated by OriginLab dose response curve fitting.

Results and discussion

The materials in the studies reported here involve photoinitiated thiol–ene chemistry, in both macroscopic gels and the microfabricated square plate system. To first establish the reaction parameters and physiochemical properties of the materials, macroscopic hydrogels were formed. The radical mediated thiol-norbornene reaction was performed with varying concentration of prepolymer solution in water from 2.5 weight percent up to 25 weight percent in 1 cm by 1 cm square molds (shown in Fig. S1†). Ethanol was later used for gel for-
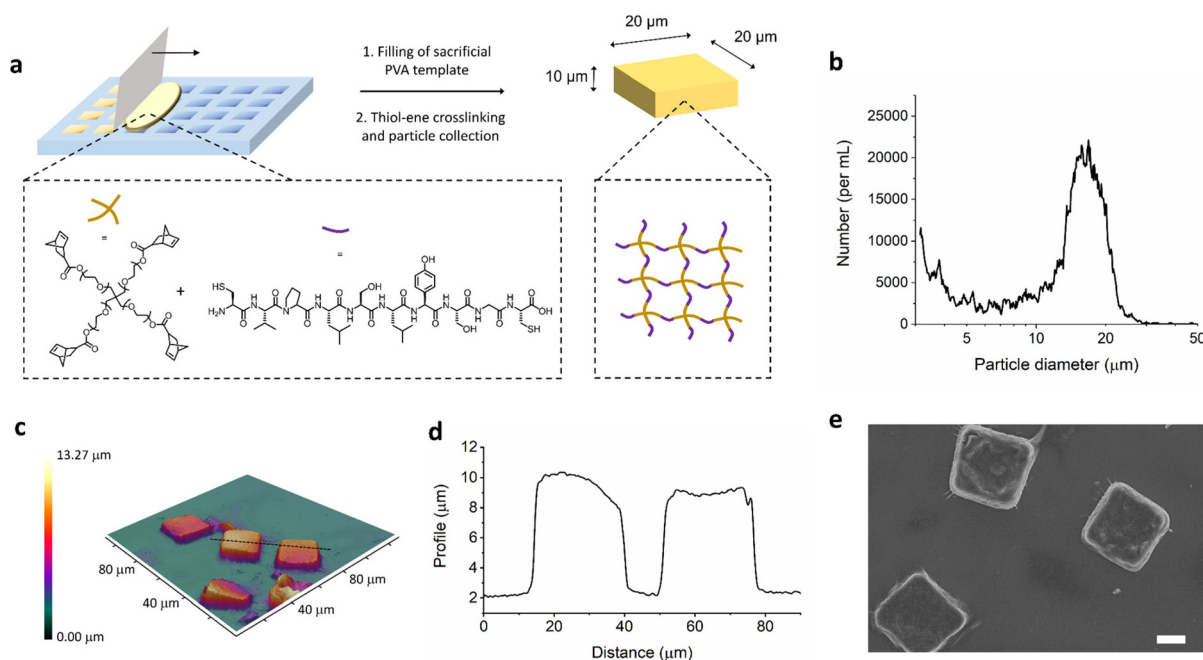
mation in lithography templates. Multifunctional 4-arm polyethylene glycol with norbornene end groups was chosen as a biocompatible network forming polymer and crosslinked with dithiol peptide (Fig. 1). The peptide, CVPLS↓LYSGC, was employed as this has previously been optimized to have a aminoacidic sequence with higher cleavage selectivity for MMP-9.[22] The thiol–ene/yne reaction allows rapid crosslinking with UV light with high selectivity and efficiency; the polymer network structure is thus very uniform and properties such as compression modulus and pore size can be easily controlled.[23–27] In Fig. S2,† we can see SEM images of the lyophilized macroscale hydrogels at different initial crosslinking concentrations.

In order to transfer this thiol–ene hydrogel crosslinking reaction to a process able to engineer the size and shape of the materials, we employed an established soft lithography templating technique (Fig. 1a).[28] This allows for the formation of polymer nanoconstructs with a size and shape depending on the design of the silicon master template which is etched with a direct laser writing device, as previously reported.[21,29–33] Further details of the templating process can be found in the ESI (Fig. S3).† Investigation of these size, shape, and stiffness properties has led to a number of key insights into particle interaction with the innate immune system,[29] biodistribution,[34] and flow properties.[35] Although, the PEG-peptide thiol–ene hydrogel system has been established for a number of years by the Anseth group,[23] it has yet to be employed to form anisotropic hydrogel particles with controlled size and shape to the best of our knowledge.

While the silicon master template has square features of 20 µm by 20 µm with a depth of 10 µm, by employing optical profilometry we can obtain information about the particles obtained after fabrication and collection from the sacrificial PVA template (Fig. 1c and d). The obtain sizes from profilometry match well with the expected sizes, confirming microplate formation. Use of the multisizer instrument allows analysis of the particle size distribution, which can be seen in Fig. 1b. The peak at around 15–20 µm is unimodal, indicating a single species. This is smaller than the longest edge of the microplates due to the non-spherical nature of the microplates being analysed as an average size. In addition, the size of hydrogel microparticles is typically underestimated by multisizer due to the particle absorbing a quantity of electrolyte and thus affecting the volume of electrolyte displaced through the instrument measurement capillary.[36] Microplate production yielding was determined as the number of collected µPLs over the total number of available wells in the template, as a percentage. This was calculated with both multisizer coulter counter and optical microscopy image analysis. Under the conditions described here, about 4×10^5 µPLs were fabricated out of 4 templates, with a yield of around 30%.

The mechanical stiffness of the hydrogels was evaluated on the macroscale formulations with compression testing. Varying the initial prepolymer solution from 2.5–25 wt% concentration led to an increase in uniaxial compression modulus from 6.5 ($n = 5$, SD 0.49) to 19.0 kPa ($n = 5$, SD 2.41), Fig. 2a

22 | *RSC Appl. Polym.*, 2023, **1**, 19–29

© 2023 The Author(s). Published by the Royal Society of Chemistry

Fig. 1 microPlates fabrication and morphological properties. (a) Brief schematic diagram of the sacrificial template soft lithography method used to produce well defined microparticles and chemical structures of polyethylene glycol hydrogels through a radical mediated thiol–ene addition mechanism, using an MMP-2/9 degradable peptide based crosslinker, (b) size distribution of microplates in aqueous solution from multisizer coulter counter, (c) optical profilometry of surface deposited microplates, (d) profile of microplates from optical profilometry, (e) SEM images of hydrogel microplates (scale bar : 10 μm).
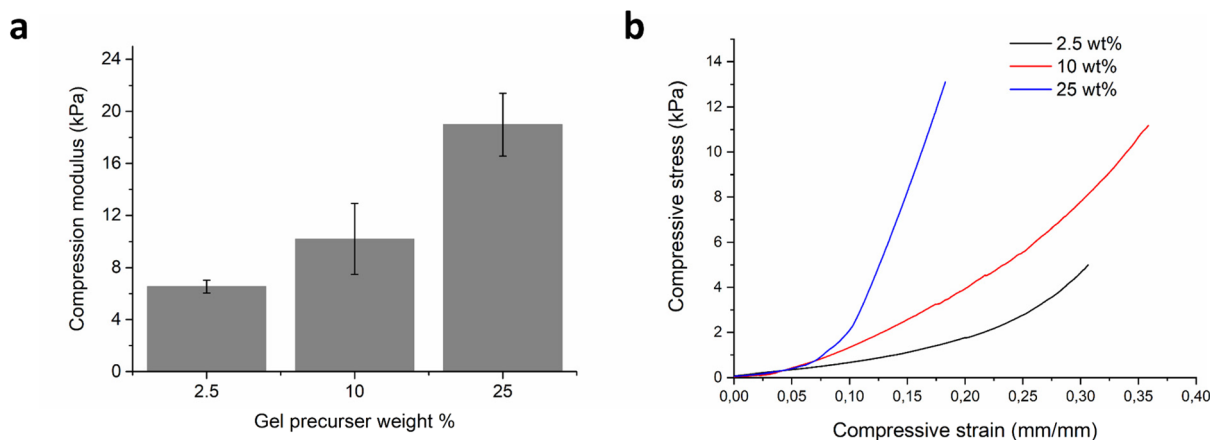
Fig. 2 Mechanical characterizations. (a) Compression moduli of macroscopic hydrogels of varying stiffness, from different gel precursor initial concentrations (error bar is S.D. of three measurements), (b) representative stress–strain curves of macroscopic hydrogels of varying stiffness, from different gel precursor initial concentrations, compression moduli taken from linear region and is the average of five samples.

and b. The equilibrium hydrogel mass swelling ratio was found to be inversely proportional to the mechanical stiffness of the hydrogels (Fig. S4†). The 2.5 wt% hydrogel had an equilibrium mass swelling ratio, Q_M, of 43.8 (n = 3, SD 4.89), the 10 wt% hydrogel 27.9 (n = 3, SD 2.61), and the most stiff 25 wt% hydrogel had an equilibrium mass swelling ratio of 16.4 (n = 3, SD 1.24). From the observed decrease in swelling, with increasing solids content in the precursor mixture, we

can also infer higher crosslinking density.[37] Similarly to the macroscopic hydrogels, the microplate polymer networks were also expected to swell when immersed in an aqueous environment. This was confirmed with optical microscopy, as seen in Fig. S5,† which gave values for fold-swelling increase, of 26.37 for the 10 wt% microplates, which is similar to the 10 wt% hydrogel value of mass swelling ratio, Q_M = 27.9, and volume swelling ratio, Q_V = 31.1. Based on these data, we decided to

© 2023 The Author(s). Published by the Royal Society of Chemistry

*RSC Appl. Polym.*, 2023, **1**, 19–29 | **23**

continue with just the one stiffness microplate made from 10 wt% precursers, as it seemed to be the best compromise between softness and swelling.

The mass degradation of the synthesized macroscale hydrogels was monitored in the presence of collagenase type IV at 37 °C (Fig. 3a and b). Collagenase type IV is a mixture of MMP-2 and MMP-9, and is representative of the highly invasive MMP rich microenvironment of tumours, which overexpress these proteases to degrade the collagen-based extracellular matrix. MMPs are known to be upregulated at all stages of expression in many cancers. Patients with head and neck squamous cell carcinoma,[38] lung cancer,[39] and colorectal cancer[40] among others, are known to have higher than normal concentrations of serum MMP-9. Concentrations for the *in vitro* analysis of hydrogel degradation were chosen based on levels of MMP-2 in the extracellular tumour microenvironment being previously estimated to be approximately 1 mM.[41] Synthesized macroscale hydrogels degrade over the course of weeks in solutions of 10 nM and 50 nM collagenase, with around 60% and 40% mass remaining respectively, after seven days. In a solution of 500 nM collagenase, the hydrogel squares degrade in approximately one day, while the gels showed negligible degradation after one week incubation in PBS only. In theory, protease degradation of hydrogels can follow either a bulk degradation mechanism or surface erosion.[42] The distinction depends on both the molecular weight and size of the enzyme, and also the crosslinking density of the hydrogel. When diffusion of the exogenously added enzyme into the hydrogel is faster than peptide cleavage there will be bulk degradation, and when the cleavage is faster than protein diffusion, the degradation will follow a surface erosion mechanism. Due to

the molecular weights and sizes of most proteases being in the order of 10 s–100 s of kilodaltons and 2–20 nm, surface erosion is usually the most likely mode of gel degradation.[24,43,44] In Fig. 3a, we can see the mass degradation reaches a linear rate, after an initial non-linear region, indicating enzyme based surface erosion. In addition, the different stiffness hydrogels were characterized for their enzyme degradability in 50 nM collagenase (Fig. S6†), with the crosslinking density also playing a role in degradation kinetics.

In order to compare the mass degradation of the microplates with that of the macroscopic hydrogels, a degradation assay was carried out in different concentrations of enzyme solution (Fig. 3c and d). The rates of degradation are faster in the case of microplates in the same concentrations of enzyme. This is expected as the degradation will occur *via* surface erosion, therefore the effect of increased surface area on degradation rate can be seen at the investigated concentrations. Additional qualitative visual confirmation of the microplate degradation in response to MMP enzymes was carried out with optical microscopy (Fig. S7†).

With the hydrogel microparticle fabrication protocol established and particles characterised, we progressed to incorporate the small chemotherapeutic molecule docetaxel (Fig. 4). Hydrogels have been established to be versatile materials for the controlled release of water soluble compounds.[13] When it comes to hydrophobic compounds, like much of the chemotherapeutics and imaging agents currently available, typically researchers introduce a nanoparticle to encapsulate the desired compounds and provide solubility and retention in the hydrophilic polymer matrix.[45] Drug release from these hierarchical systems have two main routes, the slow release of
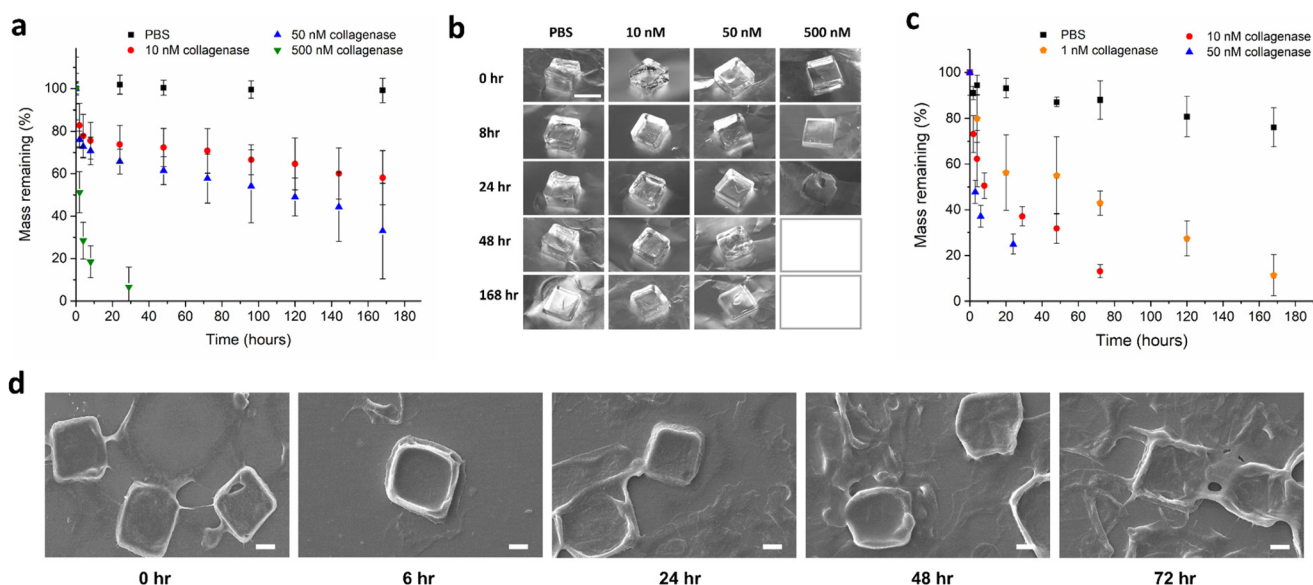
Fig. 3 Biodegradation studies. (a) Macroscopic gel (10 wt% precursors) mass degradation in varying concentrations of MMP-2/9 (collagenase IV) at 37 °C over time, (b) images of macroscale hydrogels (1 cm × 1 cm) at varying points of degradation corresponding to sampling times from panel a (scale bar: 10 mm), (c) hydrogel microplate mass degradation in varying concentrations of MMP-2/9 (collagenase IV) at 37 °C over time, (d) SEM images of hydrogel microplates and their degradation in 10 nM of MMP-2/9 (collagenase IV) at 37 °C, over time (scale bars: 10 μm).
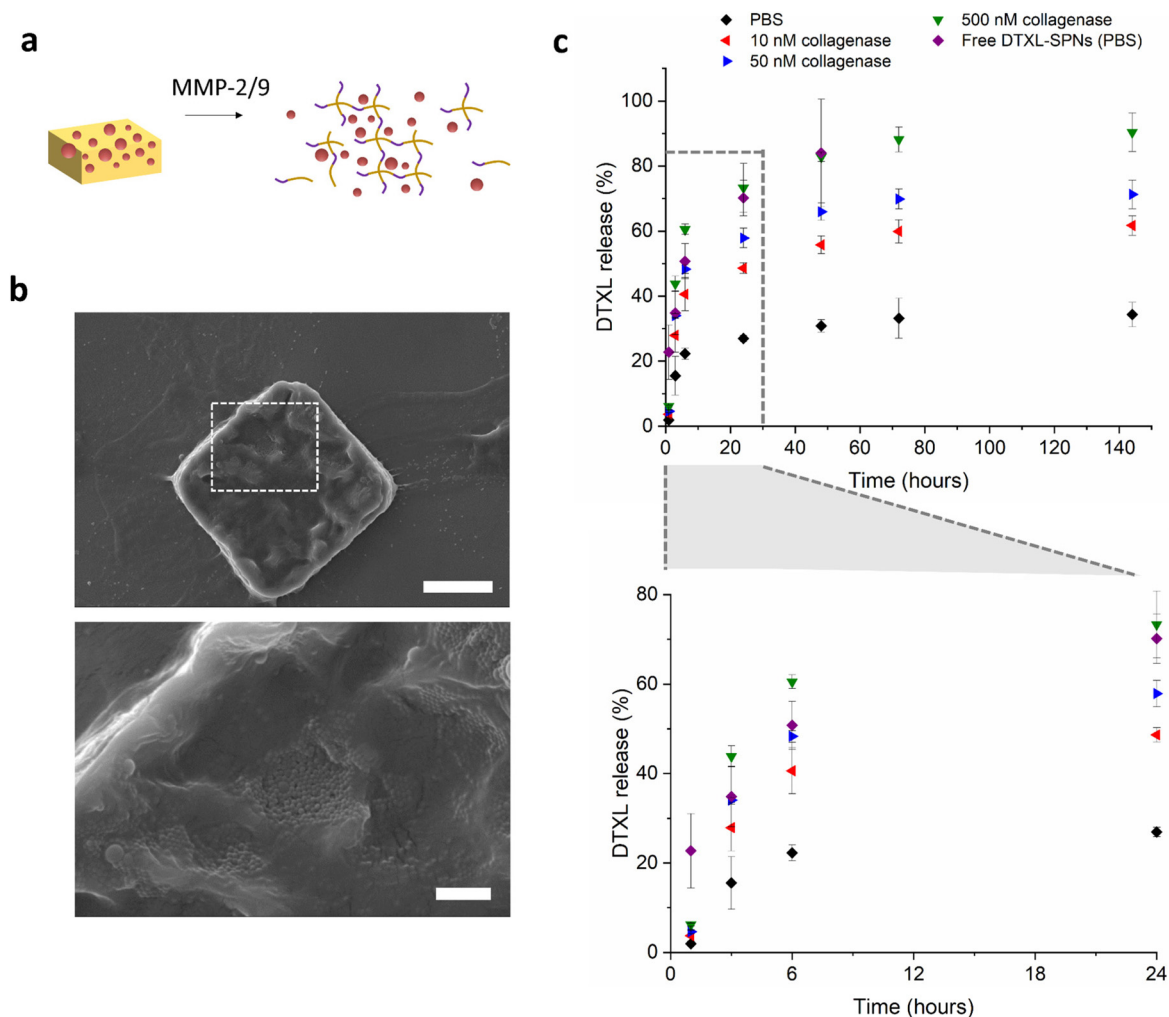
Fig. 4 Drug loading and release. (a) Schematic of the degradation of DTXL containing SPN loaded microplates in MMP-2/9 (collagenase IV), (b) SEM images of surface deposited hydrogel microplates loaded with DTXL-containing PLGA SPNs, (c) release profiles of DTXL from SPN-loaded microplates quantified by HPLC. Scale bars: 10 μm (top) and 2 μm (bottom).

drug-loaded particles from the hydrogel and subsequent release of the therapeutic from the nanoparticles, or alternatively, there could be release of the drug from the nanoparticles inside the gel and then diffusion of the drug molecules through the hydrogel network. There is also a third case, in which the drug is released *via* a combination of these mechanisms.[46,47] Which mechanism dominates can be due to various factors such as particle size, nature of the incorporated drug molecule, hydrogel network size, and chemical composition of the hydrogel and particle.

Poly(DL-lactic-*co*-glycolic acid) (PLGA) spherical nanoparticles (SPNs) were formed *via* an oil in water solvent evaporation method, and encapsulated docetaxel. The physiochemical properties of the SPNs were measured by dynamic light scattering, and the intensity averaged diameter was found to be around 200 nm and the zeta potential −45 mV (Fig. S8a and S8b†). Encapsulation efficiency of DTXL in SPNs was 28.2% ($n = 3$, SD 7.2), and loading efficiency was 5.6% ($n = 3$, SD 0.9). Loading of the nanoparticles into the formed hydrogel

microplates was achieved following a similar protocol to that previously reported by Mooney and colleagues,[48] and also the group of Zhang.[49] Briefly, microplates were lyophilized, allowed to reswell in a small volume of concentrated SPNs for 2 hours, and the unloaded SPNs removed by addition of water and centrifugation to collect the SPN-loaded microplates. Size and morphology of the microplates were observed with SEM. Fig. 4b shows a SEM image of the loaded microplates with visible SPNs and a size of approximately 20 μm by 20 μm. After lyophilization, the microplates have a rougher surface, with features similar to the macroscopic hydrogel although not as porous. It is expected that while there are some surface adsorbed SPNs, there will also be a significant amount that will penetrate into the hydrogel during the rehydration of the lyophilized microplates. DTXL-SPN loading was confirmed quantitatively with HPLC, which gave values for encapsulation efficiency of SPNs into microplates of EE = 35%, ($n = 3$, SD 6.1) and overall DTXL loading efficiency into microplates of LE = 2.0% ($n = 3$, SD 0.4).

© 2023 The Author(s). Published by the Royal Society of Chemistry

*RSC Appl. Polym.*, 2023, **1**, 19–29 | **25**

The kinetics of docetaxel release from MMP responsive microplates was monitored with HPLC under various representative physiological conditions at 37 °C, and is shown in Fig. 4c. In PBS, the release of docetaxel reaches 20% after 6 hours, and then the release rate enters a second slower phase, with approximately 30–35% drug release after 6 days. When incubated in simulated tumour environments, with different concentrations of MMPs at 37 °C, the drug release is faster. With an enzyme concentration of 10 nM, a 50% docetaxel release is achieved after one day, which then slows to reach 60% after 6 days. In the presence of 50 nM collagenase IV, the drug release is 55–60% after 1 day, and 70% after 6 days. In the 500 nM enzyme concentration case, most representative of the high concentrations of MMPs expected in the microenvironment of infiltrating tumours, there is approximately 75% drug release after one day reaching 90% after 3 days. This release profile overlaps with the release profile of DTXL from free SPNs (not embedded in the μPL), indicating that the hydrogel matrix is being degraded faster than the drug is being released from the PLGA SPNs. In the conditions with less than 500 nM collagenase, the release of DTXL from the μPL is slower than the release from free SPNs, suggesting that the presence of the hydrogel network (and potentially the interactions with the peptides) slow down the release. In addition, the nonlinear shape of the release profiles is likely due to a combination of modes of release. The initial faster

release is likely due to release of particles from the microplates which then release drug as free SPNs, while the remaining encapsulated SPNs could be releasing drug inside the microplates, which then diffuses out at a slower rate.

The performance of MMP-μPL carrying DTXL-SPN (DTXL-MMP-μPL) *in vitro* was studied with the aggressive and rapidly proliferating U87-MG glioma cells, which are known to overexpress matrix metalloproteinases (Fig. 5). Expression of MMPs by U87-MG cells was confirmed by a commercial FRET-based quantification kit and was found to be approximately 10 nM in the cell media. Both MMP responsive and nonresponsive empty μPLs were found to be nontoxic to U87-MG cells even at a high concentration, indicating good biocompatibility of these materials as nanoparticle or drug depots (Fig. 5b). When loaded with drug containing nanoparticles, DTXL-MMP-μPL, reduced the viability of U87-MG cells to 40% at an overall DTXL concentration of 50 nM (EC_{50} = 1.88 nM), indicating a potent anti-tumor effect. Without the MMP degradable cross-linker, *i.e.* non-responsive to the tumour microenvironment, the DTXL-μPL, triggered a significantly lower cytotoxicity, quantifiable by an over 20-fold increase in EC_{50} compared to the MMP degradable system. The effect of MMP degradable linkers can also be seen qualitatively with optical microscopy when DTXL-MMP-μPL and DTXL-μPL, were imaged following 48 h incubation with U87-MG cells (Fig. 5e). When equal numbers of microplates are incubated with cells, the peptide
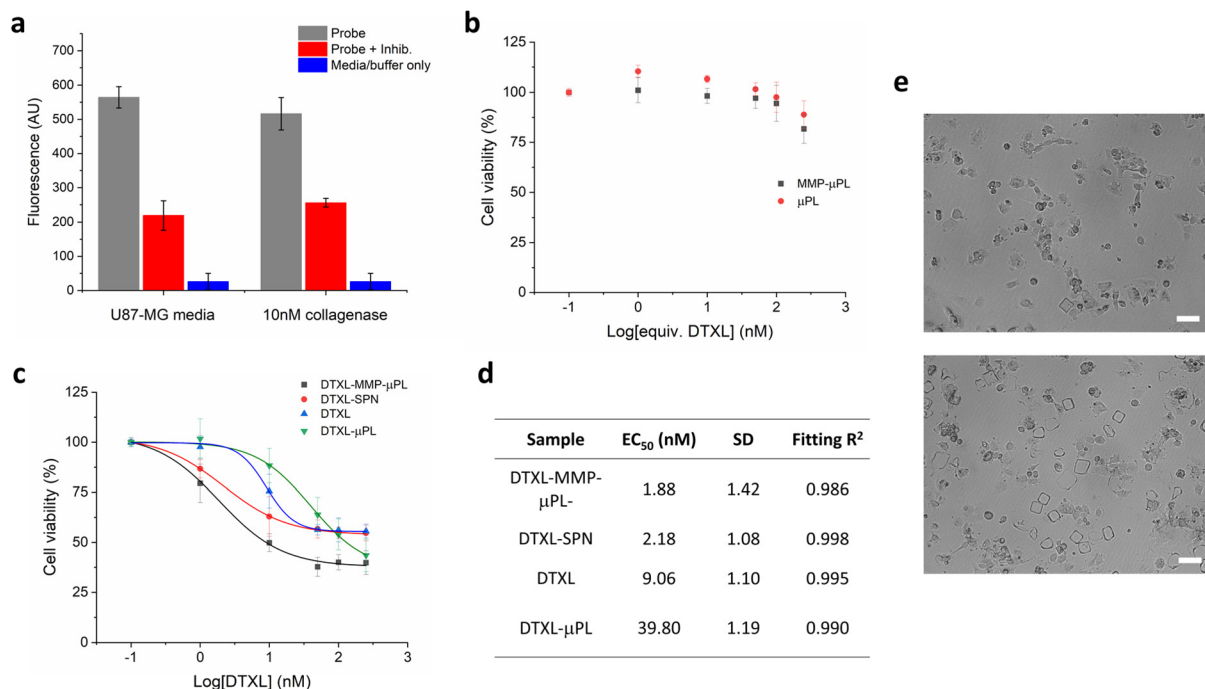
Fig. 5 Cytotoxicity on cancer cells. (a) FRET probe based collagenase IV (MMP-2/9) enzymatic activity assay, conducted with culture media after 24 h culture with cells, compared to 10 nM collagenase IV control solution (inhibitor from supplied kit, Merck InnoZyme), (b) MTT assays of various microplate treatment options (U87-MG cells) at 72 h (non-loaded microplates at the same particle concentration as used in the DTXL containing samples), (c) MTT assays of various microplate treatment options (U87-MG cells) at 72 h, (d) fitted dose response curve EC_{50} values from various treatment groups, (e) brightfield microscopy images of U87-MG (7500 cells per well), after 48 h of exposure to MMP degradable (top) or non-degradable (bottom) μPL containing DTXL SPNs, EMEM medium, 100 nM total DTXL concentration. Scale bars: 100 μm.

crosslinked microplates are reduced in number compared to non-degradable dithiothreitol (DTT) crosslinked microplates. Accordingly, more marked signs of cell morphology alterations and cell death could be observed upon the treatment with DTXL-MMP-µPL due to the selective release of DTXL. This confirms the greater efficacy of DTXL-MMP-µPL is likely due to the MMP degradable hydrogel microplates, and that targeting the tumour microenvironment is an effective strategy to increase therapeutic efficacy. Taken together, these results show that DTXL-MMP-µPL gives a safe, tumour microenvironment specific, and highly effective antitumor treatment in this invasive cell-line model. Future studies could look to further validate these results *in vivo*, in a relevant tumour model, either glioblastoma derived or otherwise. Another interesting avenue for research would be the variation of hydrogel microplate size, which could lead to different rates of nanoparticle release for different size microgels based on relative surface area differences.

Conclusions

To summarise, we have developed an enzyme responsive hierarchical microparticle system for tumour microenvironment targeting, with chemotherapeutic docetaxel for the improved treatment of invasive tumour cells. The specific design parameters including size, shape, and mechanical stiffness, combined with MMP-2/9 responsive crosslinks will allow docetaxel containing nanoparticles to be released at the infiltrating tumour edge where the concentration of MMPs is high. This cell-responsive interactive material has a number of potential advantages for glioblastoma treatment, (i) pre-engineered microparticle scaffolds allow injectability and also a tunable stiffness to better interact with the surrounding tissue, (ii) the MMP degradable polymer material increases docetaxel dosage in a spatiotemporally controlled manner in response to tumour cells, (iii) the hierarchical nature by including docetaxel containing nanoparticles, delays diffusion of drug from hydrogel microplates and increases cellular accumulation by having a multistage type device. This new multifunctional nanomedicine platform is an effective and versatile system for treatment of invasive MMP expressing cells. In the future, the system could incorporate further imaging modalities, or additional therapeutics, and is thus a promising material for the treatment of cancer.

Conflicts of interest

There are no conflicts to declare.

Acknowledgements

References

1 E. C. Holland, Glioblastoma Multiforme: The Terminator, *Proc. Natl. Acad. Sci. U. S. A.*, 2000, **97**(12), 6242–6244, DOI: **10.1073/pnas.97.12.6242**.

2 K. J. Wolf, J. Chen, J. D. Coombes, M. K. Aghi and S. Kumar, Dissecting and Rebuilding the Glioblastoma Microenvironment with Engineered Materials, *Nat. Rev. Mater.*, 2019, **4**(10), 651–668, DOI: **10.1038/s41578-019-0135-y**.

3 A. F. Tamimi and M. Juweid, Epidemiology and Outcome of Glioblastoma, in *Glioblastoma*, ed. S. De Vleeschouwer, Codon Publications, Brisbane (AU), 2017.

4 R. Stupp, W. P. Mason, M. J. van den Bent, M. Weller, B. Fisher, M. J. B. Taphoorn, K. Belanger, A. A. Brandes, C. Marosi, U. Bogdahn, J. Curschmann, R. C. Janzer, S. K. Ludwin, T. Gorlia, A. Allgeier, D. Lacombe, J. G. Cairncross, E. Eisenhauer and R. O. Mirimanoff, Radiotherapy plus Concomitant and Adjuvant Temozolomide for Glioblastoma, *N. Engl. J. Med.*, 2005, **352**(10), 987–996, DOI: **10.1056/NEJMoa043330**.

5 O. Gallego, Nonsurgical Treatment of Recurrent Glioblastoma, *Curr. Oncol.*, 2015, **22**(4), 273–281, DOI: **10.3747/co.22.2436**.

6 J. Guo, M. Schlich, J. F. Cryan and C. M. O'Driscoll, Targeted Drug Delivery via Folate Receptors for the Treatment of Brain Cancer: Can the Promise Deliver?, *J. Pharm. Sci.*, 2017, **106**(12), 3413–3420, DOI: **10.1016/j.xphs.2017.08.009**.

7 L.-L. Bu, J. Yan, Z. Wang, H. Ruan, Q. Chen, V. Gunadhi, R. B. Bell and Z. Gu, Advances in Drug Delivery for Post-Surgical Cancer Treatment, *Biomaterials*, 2019, **219**, 119182, DOI: **10.1016/j.biomaterials.2019.04.027**.

8 Q. Chen, C. Wang, X. Zhang, G. Chen, Q. Hu, H. Li, J. Wang, D. Wen, Y. Zhang, Y. Lu, G. Yang, C. Jiang, J. Wang, G. Dotti and Z. Gu, In Situ Sprayed Bioresponsive Immunotherapeutic Gel for Post-Surgical Cancer Treatment, *Nat. Nanotechnol.*, 2019, **14**(1), 89–97, DOI: **10.1038/s41565-018-0319-4**.

9 A. Bregy, A. H. Shah, M. V. Diaz, H. E. Pierce, P. L. Ames, D. Diaz and R. J. Komotar, The Role of Gliadel Wafers in the Treatment of High-Grade Gliomas, *Expert Rev. Anticancer Ther.*, 2013, **13**(12), 1453–1461, DOI: **10.1586/14737140.2013.840090**.

10 H. J. Busscher, H. C. van der Mei, G. Subbiahdoss, P. C. Jutte, J. J. A. M. van den Dungen, S. A. J. Zaat, M. J. Schultz and D. W. Grainger, Biomaterial-Associated Infection: Locating the Finish Line in the Race for the Surface, *Sci. Transl. Med.*, 2012, **4**(153), 153rv10, DOI: **10.1126/scitranslmed.3004528**.

11 A. M. Kloxin, C. J. Kloxin, C. N. Bowman and K. S. Anseth, Mechanical Properties of Cellularly Responsive Hydrogels

and Their Experimental Determination, *Adv. Mater.*, 2010, **22**(31), 3484–3494, DOI: **10.1002/adma.200904179**.

12 F. Chambon and H. H. Winter, Linear Viscoelasticity at the Gel Point of a Crosslinking PDMS with Imbalanced Stoichiometry, *J. Rheol.*, 1987, **31**(8), 683–697, DOI: **10.1122/1.549955**.

13 J. Li and D. J. Mooney, Designing Hydrogels for Controlled Drug Delivery, *Nat. Rev. Mater.*, 2016, **1**(12), 1–17, DOI: **10.1038/natrevmats.2016.71**.

14 Y. S. Zhang and A. Khademhosseini, Advances in Engineering Hydrogels, *Science*, 2017, **356**(6337), eaaf3627, DOI: **10.1126/science.aaf3627**.

15 A. B. Cook and P. Decuzzi, Harnessing Endogenous Stimuli for Responsive Materials in Theranostics, *ACS Nano*, 2021, **15**(2), 2068–2098.

16 C. Bastiancich, J. Bianco, K. Vanvarenberg, B. Ucakar, N. Joudiou, B. Gallez, G. Bastiat, F. Lagarce, V. Préat and F. Danhier, Injectable Nanomedicine Hydrogel for Local Chemotherapy of Glioblastoma after Surgical Resection, *J. Controlled Release*, 2017, **264**, 45–54, DOI: **10.1016/j.jconrel.2017.08.019**.

17 D. Di Mascolo, A. L. Palange, R. Primavera, F. Macchi, T. Catelani, F. Piccardi, R. Spanò, M. Ferreira, R. Marotta, A. Armirotti, A. L. Gallotti, R. Galli, C. Wilson, G. A. Grant and P. Decuzzi, Conformable Hierarchically Engineered Polymeric Micromeshes Enabling Combinatorial Therapies in Brain Tumours, *Nat. Nanotechnol.*, 2021, **16**(7), 820–829, DOI: **10.1038/s41565-021-00879-3**.

18 M. Zhao, E. Bozzato, N. Joudiou, S. Ghiassinejad, F. Danhier, B. Gallez and V. Préat, Codelivery of Paclitaxel and Temozolomide through a Photopolymerizable Hydrogel Prevents Glioblastoma Recurrence after Surgical Resection, *J. Controlled Release*, 2019, **309**, 72–81, DOI: **10.1016/j.jconrel.2019.07.015**.

19 K. J. Isaacson, M. M. Jensen, N. B. Subrahmanyam and H. Ghandehari, Matrix-Metalloproteinases as Targets for Controlled Delivery in Cancer: An Analysis of Upregulation and Expression, *J. Controlled Release*, 2017, **259**, 62–75, DOI: **10.1016/j.jconrel.2017.01.034**.

20 S. P. Zustiak and J. B. Leach, Hydrolytically Degradable Poly(Ethylene Glycol) Hydrogel Scaffolds with Tunable Degradation and Mechanical Properties, *Biomacromolecules*, 2010, **11**(5), 1348–1357, DOI: **10.1021/bm100137q**.

21 J. Key, A. L. Palange, F. Gentile, S. Aryal, C. Stigliano, D. Di Mascolo, E. De Rosa, M. Cho, Y. Lee, J. Singh and P. Decuzzi, Soft Discoidal Polymeric Nanoconstructs Resist Macrophage Uptake and Enhance Vascular Targeting in Tumors, *ACS Nano*, 2015, **9**(12), 11628–11641, DOI: **10.1021/acsnano.5b04866**.

22 J. Patterson and J. A. Hubbell, Enhanced Proteolytic Degradation of Molecularly Engineered PEG Hydrogels in Response to MMP-1 and MMP-2, *Biomaterials*, 2010, **31**(30), 7836–7845, DOI: **10.1016/j.biomaterials.2010.06.061**.

23 B. D. Fairbanks, M. P. Schwartz, A. E. Halevi, C. R. Nuttelman, C. N. Bowman and K. S. Anseth, A Versatile Synthetic Extracellular Matrix Mimic via Thiol-Norbornene Photopolymerization, *Adv. Mater.*, 2009, **21**(48), 5005–5010, DOI: **10.1002/adma.200901808**.

24 A. A. Aimetti, A. J. Machen and K. S. Anseth, Poly(Ethylene Glycol) Hydrogels Formed by Thiol-Ene Photopolymerization for Enzyme-Responsive Protein Delivery, *Biomaterials*, 2009, **30**(30), 6048–6054, DOI: **10.1016/j.biomaterials.2009.07.043**.

25 A. B. Cook, R. Barbey, J. A. Burns and S. Perrier, Hyperbranched Polymers with High Degrees of Branching and Low Dispersity Values: Pushing the Limits of Thiol–Yne Chemistry, *Macromolecules*, 2016, **49**(4), 1296–1304, DOI: **10.1021/acs.macromol.6b00132**.

26 M. Hartlieb, T. Floyd, A. B. Cook, C. Sanchez-Cano, S. Catrouillet, J. A. Burns and S. Perrier, Well-Defined Hyperstar Copolymers Based on a Thiol–Yne Hyperbranched Core and a Poly(2-Oxazoline) Shell for Biomedical Applications, *Polym. Chem.*, 2017, **8**(13), 2041–2054, DOI: **10.1039/C7PY00303J**.

27 A. B. Cook, R. Peltier, J. Zhang, P. Gurnani, J. Tanaka, J. A. Burns, R. Dallmann, M. Hartlieb and S. Perrier, Hyperbranched Poly(Ethylenimine-Co-Oxazoline) by Thiol–Yne Chemistry for Non-Viral Gene Delivery: Investigating the Role of Polymer Architecture, *Polym. Chem.*, 2019, **10**(10), 1202–1212, DOI: **10.1039/C8PY01648H**.

28 D. A. Canelas, K. P. Herlihy and J. M. DeSimone, Top-down Particle Fabrication: Control of Size and Shape for Diagnostic Imaging and Drug Delivery, *Wiley Interdiscip. Rev.: Nanomed. Nanobiotechnol.*, 2009, **1**(4), 391–404, DOI: **10.1002/wnan.40**.

29 R. Palomba, A. L. Palange, I. F. Rizzuti, M. Ferreira, A. Cervadoro, M. G. Barbato, C. Canale and P. Decuzzi, Modulating Phagocytic Cell Sequestration by Tailoring Nanoconstruct Softness, *ACS Nano*, 2018, **12**(2), 1433–1444, DOI: **10.1021/acsnano.7b07797**.

30 A. B. Cook, M. Schlich, P. N. Manghnani, T. L. Moore, P. Decuzzi and A. L. Palange, Size Effects of Discoidal PLGA Nanoconstructs in Pickering Emulsion Stabilization, *J. Polym. Sci.*, 2022, **60**(9), 1480–1491, DOI: **10.1002/pol.20210748**.

31 A. B. Cook and T. D. Clemons, Bottom-Up versus Top-Down Strategies for Morphology Control in Polymer-Based Biomedical Materials, *Adv. NanoBiomed Res.*, 2022, **2**(1), 2100087, DOI: **10.1002/anbr.202100087**.

32 M. Di Francesco, R. Primavera, D. Romanelli, R. Palomba, R. C. Pereira, T. Catelani, C. Celia, L. Di Marzio, M. Fresta, D. Di Mascolo and P. Decuzzi, Hierarchical Microplates as Drug Depots with Controlled Geometry, Rigidity, and Therapeutic Efficacy, *ACS Appl. Mater. Interfaces*, 2018, **10**(11), 9280–9289, DOI: **10.1021/acsami.7b19136**.

33 T. L. Moore, A. B. Cook, E. Bellotti, R. Palomba, P. Manghnani, R. Spanò, S. Brahmachari, M. Di Francesco, A. L. Palange, D. Di Mascolo and P. Decuzzi, Shape-Specific Microfabricated Particles for Biomedical Applications: A Review, *Drug Delivery Transl. Res.*, 2022, **12**(8), 2019–2037, DOI: **10.1007/s13346-022-01143-4**.

34 P. Decuzzi, B. Godin, T. Tanaka, S.-Y. Lee, C. Chiappini, X. Liu and M. Ferrari, Size and Shape Effects in the Biodistribution of Intravascularly Injected Particles, *J. Controlled Release*, 2010, **141**(3), 320–327, DOI: **10.1016/j.jconrel.2009.10.014**.

35 P. Decuzzi, R. Pasqualini, W. Arap and M. Ferrari, Intravascular Delivery of Particulate Systems: Does Geometry Really Matter?, *Pharm. Res.*, 2009, **26**(1), 235–243, DOI: **10.1007/s11095-008-9697-x**.

36 M. Pellegrini, A. Cherukupalli, M. Medini, R. Falkowski and R. Olabisi, The Effect of Swelling Ratio on the Coulter Underestimation of Hydrogel Microsphere Diameters, *Tissue Eng., Part C*, 2015, **21**(12), 1246–1250, DOI: **10.1089/ten.tec.2015.0246**.

37 T. Canal and N. A. Peppas, Correlation between Mesh Size and Equilibrium Degree of Swelling of Polymeric Networks, *J. Biomed. Mater. Res.*, 1989, **23**(10), 1183–1193, DOI: **10.1002/jbm.820231007**.

38 F. Riedel, K. Götte, J. Schwalb and K. Hörmann, Serum Levels of Matrix Metalloproteinase-2 and -9 in Patients with Head and Neck Squamous Cell Carcinoma, *Anticancer Res.*, 2000, **20**(5A), 3045–3049.

39 E. Hrabec, M. Strek, D. Nowak and Z. Hrabec, Elevated Level of Circulating Matrix Metalloproteinase-9 in Patients with Lung Cancer, *Respir. Med.*, 2001, **95**(1), 1–4, DOI: **10.1053/rmed.2000.0923**.

40 A. Jonsson, C. Hjalmarsson, P. Falk and M.-L. Ivarsson, Levels of Matrix Metalloproteinases Differ in Plasma and Serum – Aspects Regarding Analysis of Biological Markers in Cancer, *Br. J. Cancer*, 2016, **115**(6), 703–706, DOI: **10.1038/bjc.2016.127**.

41 H. Hatakeyama, H. Akita, K. Kogure, M. Oishi, Y. Nagasaki, Y. Kihira, M. Ueno, H. Kobayashi, H. Kikuchi and H. Harashima, Development of a Novel Systemic Gene Delivery System for Cancer Therapy with a Tumor-Specific Cleavable PEG-Lipid, *Gene Ther.*, 2007, **14**(1), 68–77, DOI: **10.1038/sj.gt.3302843**.

42 P. M. Kharkar, K. L. Kiick and A. M. Kloxin, Designing Degradable Hydrogels for Orthogonal Control of Cell Microenvironments, *Chem. Soc. Rev.*, 2013, **42**(17), 7335–7372, DOI: **10.1039/C3CS60040H**.

43 C.-C. Lin, C. S. Ki and H. Shih, Thiol–Norbornene Photoclick Hydrogels for Tissue Engineering Applications, *J. Appl. Polym. Sci.*, 2015, **132**(8), 41563, DOI: **10.1002/app.41563**.

44 H. Shih and C.-C. Lin, Cross-Linking and Degradation of Step-Growth Hydrogels Formed by Thiol–Ene Photoclick Chemistry, *Biomacromolecules*, 2012, **13**(7), 2003–2012, DOI: **10.1021/bm300752j**.

45 S. J. Buwalda, T. Vermonden and W. E. Hennink, Hydrogels for Therapeutic Delivery: Current Developments and Future Directions, *Biomacromolecules*, 2017, **18**(2), 316–330, DOI: **10.1021/acs.biomac.6b01604**.

46 M.-C. Chen, H.-W. Tsai, C.-T. Liu, S.-F. Peng, W.-Y. Lai, S.-J. Chen, Y. Chang and H.-W. Sung, A Nanoscale Drug-Entrapment Strategy for Hydrogel-Based Systems for the Delivery of Poorly Soluble Drugs, *Biomaterials*, 2009, **30**(11), 2102–2111, DOI: **10.1016/j.biomaterials.2008.12.047**.

47 C. Lu, R. B. Yoganathan, M. Kociolek and C. Allen, Hydrogel Containing Silica Shell Cross-Linked Micelles for Ocular Drug Delivery, *J. Pharm. Sci.*, 2013, **102**(2), 627–637, DOI: **10.1002/jps.23390**.

48 T. Bauleth-Ramos, T.-Y. Shih, M.-A. Shahbazi, A. J. Najibi, A. S. Mao, D. Liu, P. Granja, H. A. Santos, B. Sarmento and D. J. Mooney, Acetalated Dextran Nanoparticles Loaded into an Injectable Alginate Cryogel for Combined Chemotherapy and Cancer Vaccination, *Adv. Funct. Mater.*, 2019, **29**(35), 1903686, DOI: **10.1002/adfm.201903686**.

49 N. C. Grant, A. I. Cooper and H. Zhang, Uploading and Temperature-Controlled Release of Polymeric Colloids via Hydrophilic Emulsion-Templated Porous Polymers, *ACS Appl. Mater. Interfaces*, 2010, **2**(5), 1400–1406, DOI: **10.1021/am100049r**.

© 2023 The Author(s). Published by the Royal Society of Chemistry

RSC Appl. Polym., 2023, **1**, 19–29 | 29